Available online at www.sciencedirect.com

SciVerse ScienceDirect

Physics Procedia 27 (2012) 408 – 411

Physics Procedia

ISS2011

Influence analysis of structural parameters and operating parameters on electromagnetic properties of HTS linear induction motor

J. Fang*, L. Sheng, D. Li, J. Zhao, Sh. Li, W. Qin, Y. Fan, Q.L. Zheng, W. Zhang

School of Electrical Engineering, Beijing Jiaotong University, Beijing,100044, China

Abstract

A novel High Temperature Superconductor Linear Induction Motor (HTS LIM) is researched in this paper. Since the critical current and the electromagnetic force of the motor are determined mainly by the primary slot leakage flux, the main magnetic flux and eddy current respectively, in order to research the influence of structural parameters and operating parameters on electromagnetic properties of HTS LIM, the motor was analyzed by 2D transient Finite Element Method (FEM). The properties of the motor, such as the maximum slot leakage flux density, motor thrust, motor vertical force and critical current are analyzed with different structural parameters and operating parameters. In addition, an experimental investigation was carried out on prototype HTS motor. Electrical parameters were deduced from these tests and also compared with the analysis results from FEM. AC losses of one HTS coil in the motor were measured and AC losses of all HTS coils in HTS LIM were estimated. The results in this paper could provide reference for the design and research on the HTS LIM.

Keywords: HTS LIM; leakage flux, electromagnetic force; structural parameters, AC losses

1. Introduction

As a new type of urban transit medium, the linear induction motor (LIM) system offers an array of advanced new characteristics and capabilities. The advantages are shown in route planning, as LIM trains can easily negotiate steep slopes and sharp curves, leading to the construction costs reduced by smaller route clearances and tunnel cross sections [1]. However, due to the air gap of LIM being much greater than that of a rotating motor, LIM with conventional copper windings have some obvious limitations such as heavy energy consumption and low efficiency. Due to those inherent defects, the wide spread is restricted in the wheel/rail transit system. As the development of superconductor tapes, the actual existing problems may be improved by the application of Bi-2223/Ag HTS coil to primary windings of LIM. It is possible to replace copper windings with HTS windings in order to eliminate copper loss in primary windings. Until now there has been some research in the world into HTS LIM [2-9].

A 3.5 *kW* class HTS LIM was presented in this study. The properties of the motor are analyzed with different structural parameters and operating parameters. The electromagnetic force is measured and compared with the analysis results from FEM. AC losses of one HTS coil are measured and AC losses of all HTS coils in HTS LIM are estimated. This study is focused on the method for the improvement of critical current and properties of the motor.

* Corresponding author. Tel.: +86-010-51687106; fax: +86-010-51687101.
E-mail address: fangseer@sina.com.

 doi:10.1016/j.phpro.2012.03.497

2. Electromagnetic Theory of HTSLIM

According to the principle of Lorentz force，the thrust force F_x and the vertical repulsive force F_{y1} can be induced by the interaction between the current density of the secondary plate and the conjugate component of magnetic flux density (in Eq. (1-2)) [10]. The vertical attractive force F_{y2} can also be calculated from Equations (3-4) [11-13]. HTS LIM vertical force F_y is the sum of F_{y1} and F_{y2}.

$$\boldsymbol{F}_x = \frac{1}{2}\mathrm{Re}\left\{\int_S J_e \boldsymbol{B}_y^* ds\right\} \tag{1}$$

$$\boldsymbol{F}_{y1} = \frac{1}{2}\mathrm{Re}\left\{\int_S J_e \boldsymbol{B}_x^* ds\right\} \tag{2}$$

$$\boldsymbol{F}_{y2} = \frac{3}{2g}[1-\frac{(1-\mathrm{e}^{-Q})(3-\mathrm{e}^{-Q})}{2Q}]\phi_{\mathrm{m}}^2 / L_{\mathrm{m}} \tag{3}$$

$$Q = lR_{\mathrm{r}} / (L_{\mathrm{m}} + L_{\mathrm{lr}}) \tag{4}$$

where J_e, $\boldsymbol{B}_x$, $\boldsymbol{B}_y$, ϕ_m, L_{m}, L_{lr}, R_r, l are the current density, magnetic field in the horizontal direction, magnetic field in the vertical direction, the main flux of motor, the magnetizing inductance, the leakage inductance, the resistance of secondary plate, and the motor length respectively.

The developed HTS LIM is composed of Bi-2223/Ag HTS coils cooled by liquid nitrogen. Fig.1 shows a schematic diagram of HTS LIM, of which the major specifications are summarized in Table 1. Fig.2 shows the cross-section of the motor, where HTS primary coils consist of 12 double-pancakes with racetrack shapes. The primary coils are arranged in 26 slots made of silicon steel. The primary section of HTS LIM, including the core and the coils, is placed in the cryostat filled with liquid nitrogen. Fig.3 shows the relationship between critical current and background magnetic field of HTS tape. The perpendicular field has a greater influence on critical current. The parallel field can be ignored when HTS motor is designed.

Table 1 Main design parameters of HTS LIM

Rating Power:	3.5kW	Pole pitch: τ	0.1266(m)
Number of phases: m	3	Air gap: δ	0.009(m)
Turns of primary windings: w	254	Thickness of secondary conductor: Δ	0.003 (m)
Number of primary slots: Q1	26	Thickness of secondary back iron: *hb*	0.008(m)
Slot width: *bs*	0.034(m)	Slot height: *hs*	0.0408(m)

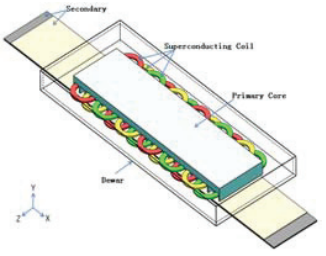

Fig. 1 Schematic diagram of HTS LIM;

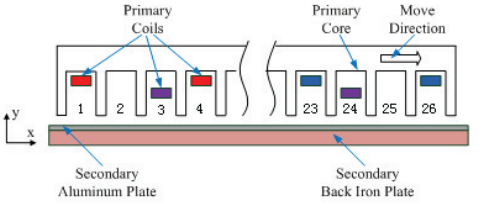

Figure 2 Cross-section of HTS LIM

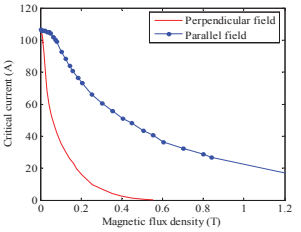

Figure 3 Critical current vs. the magnetic flux density of Bi-2223/Ag

3. FEM analysis of HTSLIM

By using ANSOFT Software, the performance of HTSLIM is well analyzed. The final optimal design parameters of the model are summarized in Table 1. Fig. 4(a) shows the relationship between thrust force and slip. The thrust force will be decreased with the electromagnetic air gap g_m. Fig. 4(b) shows the relationship between vertical force and slip. The vertical force will be decreased with g_m. It is different from the thrust force that the vertical force will be greater with the increase of motor speed. g_m is the sum of the thickness of the Dewar h_d, the mechanical air gap δ and the thickness of secondary aluminium plate Δ ($\delta = 10mm$ and $\Delta = 3mm$). In order to decrease g_m, Dewar must be thin. The designed minimum of h_d is about $9mm$ so that the designed minimum value of g_m is $21mm$.

The electromagnetic force will not be significantly influenced by different slot heights [14]. Therefore, the relationship between the electromagnetic force and the slot width is researched. Fig. 5(a) and Fig. 5(b) show thrust force and vertical force decrease with the slot width *bs*. When the slot width *bs* is increased from 47.2*mm* to 72.2*mm*, the relationship between electromagnetic force and slip is as shown in Fig. 5. Fig. 5(a) shows the greatest difference of thrust force is generated at the starting time of the motor and is about 385N. The thrust force difference will be smaller with the increase of the motor speed. Fig. 5(b) shows the greatest difference of vertical force is generated at *s*=0.5 and is about 1084N. The vertical force difference will decrease with the motor speed when slip is greater than 0.5.

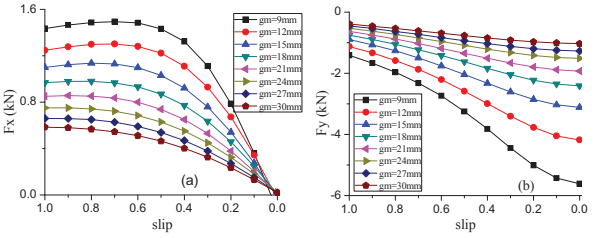

Fig.4 Electromagnetic force vs. slip with different the gap (a) shows thrust force F_x vs. the slip. (b) shows vertical force F_y vs. the slip.

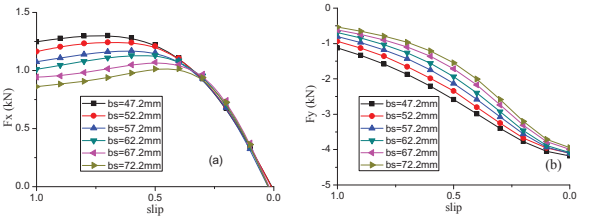

Fig.5 Electromagnetic force vs. slip with different the slot width (a) shows thrust force F_x vs. slip. (b) shows vertical force F_y vs. slip.

The slot leakage flux density, B⊥max is almost the perpendicular field. In order to increase critical current, B⊥max must be reduced as much as possible. Fig. 6 shows a three-dimensional waveform of B⊥max with different slot heights *hs*. Fig. 6 and Fig.7 show B⊥max will be reduced from 0.22 *T* to 0.184 *T* and the critical current will be increased from 20*A* to 26.7*A* when the slot height *hs* is increased from 32*mm* to 82*mm*. If the slot height is more than 62*mm*, the critical current is almost the same. A slot height such as 62 *mm* is called as a critical slot height.

Fig.8 and Fig. 9 shows B⊥max will be reduced from 0.165T to 0.117T and the critical current will be increased from 24.1A to 29.4A when the slot width *bs* is increased from 47.2 *mm* to 72.2*mm*. If the slot height is more than 72.2*mm*, the critical current is almost the same. A slot width such as 72.2*mm* is called as a critical slot width. Therefore, the critical current of the motor can be increased by using critical slot height and critical slot width.

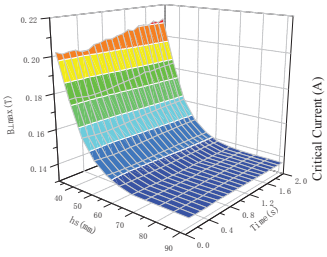

Fig.6 3D transient waveform of B⊥max with different slot height

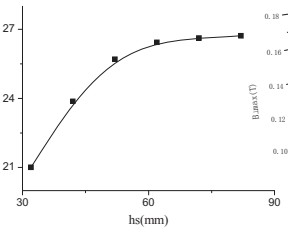

Fig.7 Critical current changing with different slot height

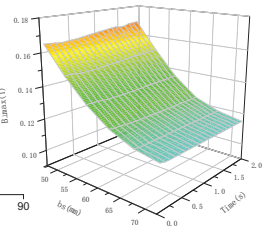

Fig.8 3D transient waveform of B⊥max with different slot width

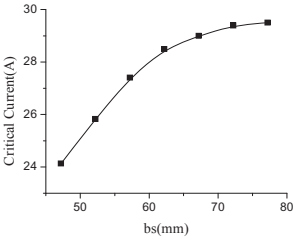

Fig.9 Critical current changing with different slot width

4. Comparison with test results

In order to design HTS LIM, a prototype motor with copper coils was designed and measured [14]. The simulation results of FEM $\boldsymbol{F}_{Mx}$ were obtained with the same conditions as the experiments and the stimulated thrust $\boldsymbol{F}_{Mx}$ is about 1.3 times greater than thrust force $\boldsymbol{F}_x$ in the experiments. Simulation thrust correction factor k_{Fx} can be calculated by $k_{Fx}= \boldsymbol{F}_x / \boldsymbol{F}_{Mx}$ and k_{Fx} is about 0.77[14]. k_{Fx} is applied in the design of a 3.5KW HTS LIM. A design target value of $\boldsymbol{F}_x$ of HTS LIM is 1100N.

Fig.10 shows a 3.5KW HTS LIM with HTS coils in the test bed. Fig.11 shows HTS LIM internal structure. This HTS LIM is tested coupled to one load linear induction motor as shown in Fig. 10. The peak of current is 18A and the frequency of current is 3Hz (shown in Fig. 12). Fig.13 shows the simulation results of FEM $\boldsymbol{F}_{Mx}$ =1100*N* and Fig. 14 shows experimental result of the starting maximum thrust F_x is 1000*N*. Fig.12 and Fig. 14 show that experimental result of the motor thrust is about 820N when the frequency is stable. Measurement results show that the actual target thrust, 1100N is achieved basically. k_{Fx} is important and useful for correcting the simulation results.

The experimental establishment of AC losses is shown in Reference [15]. Fig. 15 describes the experimental results of AC losses of the HTS coil in different frequencies. It is clearly shown that when the transport current is equal, AC loss will gradually increase when the frequency is increased from 10.25Hz to 107.5Hz. When current is 20A and the frequency of current is 10.25Hz， AC losses of HTS coil are $4.2\times10^{-7} J/m/cycle$. Total AC losses of 12 HTS coils are about 0.0128J within 1 second and could consume about 0.128W of cooling power. Compared with the

total losses, 0.128W of cooling power is too small and can be ignored. Because the copper loss of motor with copper coils is about 17% of the total losses, if HTS coils are applied in the motor, the total losses of motor can be reduced by about 15-17% so that motor efficiency can be improved evidently.

Fig.10 Photograph of HTS LIM with HTS coils in the test bed

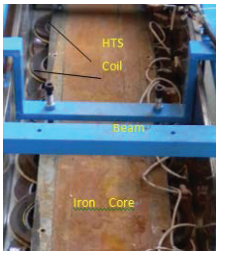

Fig.11 Photograph of HTS LIM Internal structure

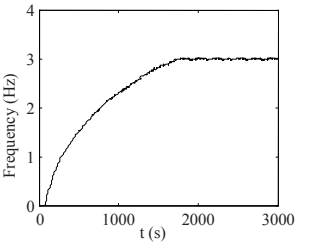

Fig.12 Frequency waveform of the HTS LIM

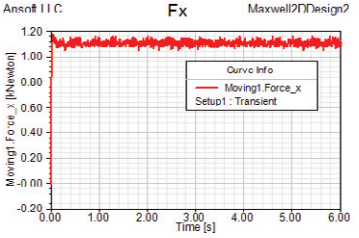

Fig.13 Simulation thrust waveform of the HTS LIM

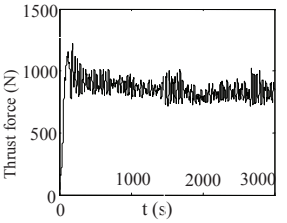

Fig.14 Experimental thrust waveform of the HTS LIM

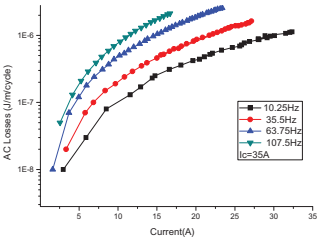

Fig.15 AC loss waveform of the HTS coil

5. Conclusions

The electromagnetic force of HTS LIM will be greater with the decrease of the gaps. The thrust force will be influenced by different slot widths and the greatest difference of thrust force is generated at the starting time of the motor. The critical current of HTS LIM is influenced by slot width and slot height and increases with slot width and slot height. Through the experimental results, the simulated thrust force can be corrected to design a new motor and the design targets of HTS LIM are achieved. AC losses of HTS coils are investigated and total AC losses of all HTS coils in HTS LIM are estimated. Motor efficiency can be improved by using superconducting motor instead of conventional motor.

Acknowledgement

This research was supported by a grant from the National High Technology Research and Development of China 863 Program (2008AA03A203).

References

[1] H. Xia, W. W. Guo, C. Y. Xia, Y. L. Pi, M. A. Bradford, Journal of Mechanical Science and Technology 23 (2009) 3257.
[2] K. Yoshida, H. Matsumoto, Physica C 392–396 (2003) 690.
[3] G. Stumberger, M. T. Aydemir, D. Zarko, T. A. Lipo, IEEE Trans. Appl. Supercond. 14 (2004) 54.
[4] K. Yoshida, H. Matsumoto, Physica C 378–381 (2002) 833.
[5] Y.G. Guo, J. X. Jin, J. G. Zhu, H. Y. Lu, IEEE Trans. Appl. Supercond. 17 (2007) 2087.
[6] H. Sugimoto, T. Tsuda, T. Morishita, Y. Hondou, T. Takeda, H. Togawa, T. Oota, , IEEE Trans. Appl. Supercond. 17 (2007) 1637.
[7] M. K. Song, S. J. Lee, Y. S. Yoon, T. K. Ko, Physica C 341–348 (2000) 2601.
[8] P. J. Masson, J. E. Pienkos, C. A. Luongo, IEEE Trans. Appl. Supercond. 17 (2007) 1579.
[9] Y. D. Jiang, R. Pei, W. Xian, Z. Hong, W. Yuan, R. Marchant, T. A. Coombs, IEEE Trans. Appl. Supercond. 19 (2009) 1644.
[10] Xialing Long, Electromagnetic Theory and Design Methods of Linear Induction Motor, China, 2006, pp. 23-24.
[11] T. Yamada, K. Fujisaki, IEEE Trans. Magnetics. 44 (2008) 4070.
[12] T. Nakamura, H. Miyake, Y. Ogama, G. Morita, I. Muta, T. Hoshino, IEEE Trans. Appl. Supercond. 16 (2006) 1469.
[13] Lee B J，Koo D H，Cho Y H． IEEE Trans. On Magnetics 45(2009)2839.
[14] J. Zhao, T.Q. Zheng, W. Zhang, J. Fang, Y.M. Liu, Physica C 471 (2011) 1474.
[15] Y. Zhao, J. Fang , W. Zhang, J. Zhao, L. Sheng, Physica C 471 (2011) 1003.